

Unimolecular decomposition of tetrazine-N-oxide based high nitrogen content energetic materials from excited electronic states

A. Bhattacharya, Y. Q. Guo, and E. R. Bernstein

Citation: *The Journal of Chemical Physics* **131**, 194304 (2009); doi: 10.1063/1.3262688

View online: <http://dx.doi.org/10.1063/1.3262688>

View Table of Contents: <http://aip.scitation.org/toc/jcp/131/19>

Published by the *American Institute of Physics*

COMPLETELY

REDESIGNED!



**PHYSICS
TODAY**

Physics Today Buyer's Guide
Search with a purpose.

Unimolecular decomposition of tetrazine-N-oxide based high nitrogen content energetic materials from excited electronic states

A. Bhattacharya, Y. Q. Guo, and E. R. Bernstein^{a)}*Department of Chemistry, Colorado State University, Fort Collins, Colorado 80523, USA*

(Received 9 June 2009; accepted 20 October 2009; published online 18 November 2009)

Unimolecular excited electronic state decomposition of novel high nitrogen content energetic molecules, such as 3,3'-azobis(6-amino-1,2,4,5-tetrazine)-mixed N-oxides (DAATO_{3,5}), 3-amino-6-chloro-1,2,4,5-tetrazine-2,4-dioxide (ACTO), and 3,6-diamino-1,2,4,5-tetrazine-1,4-dioxide (DATO), is investigated. Although these molecules are based on N-oxides of a tetrazine aromatic heterocyclic ring, their decomposition behavior distinctly differs from that of bare tetrazine, in which N₂ and HCN are produced as decomposition products through a concerted dissociation mechanism. NO is observed to be an initial decomposition product from all tetrazine-N-oxide based molecules from their low lying excited electronic states. The NO product from DAATO_{3,5} and ACTO is rotationally cold (20 K) and vibrationally hot (1200 K), while the NO product from DATO is rotationally hot (50 K) and vibrationally cold [only the (0–0) vibronic transition of NO is observed]. DAATO_{3,5} and ACTO primarily differ from DATO with regard to molecular structure, by the relative position of oxygen atom attachment to the tetrazine ring. Therefore, the relative position of oxygen in tetrazine-N-oxides is proposed to play an important role in their energetic behavior. N₂O is ruled out as an intermediate precursor of the NO product observed from all three molecules. Theoretical calculations at CASMP2/CASSCF level of theory predict a ring contraction mechanism for generation of the initial NO product from these molecules. The ring contraction occurs through an (S₁/S₀)_{CI} conical intersection. © 2009 American Institute of Physics. [doi:10.1063/1.3262688]

I. INTRODUCTION

High nitrogen content energetic materials have recently received increased attention due to their novel energetic and explosive properties.^{1–8} A high nitrogen content energetic material is a compound with a large number of N–N linkages. Increasing the nitrogen content at the expense of carbon/hydrogen content in the energetic molecule has several advantages: (1) the low percentage of carbon and hydrogen allows a good oxygen balance and increases crystal density^{1,6} and (2) utilization of the N–N moiety in the energetic species increases its heat of formation (enthalpy of formation often exceeds 400 kcal/mol).¹ These unique characteristics of nitrogen rich energetic materials are critical parameters for enhancement of their energy storage capabilities. Additionally, a high percentage of their decomposition product is expected to be the colorless, inert, nontoxic, and environmentally friendly, nitrogen molecule. These features can also facilitate the formation of smoke free, “reduced-signature” propellants which are useful for military applications. Therefore, nitrogen rich energetic materials are promising substitutes for the more traditional nitramine and nitro-containing systems and would be more acceptable than these traditional energetic materials for both industrial and military use in the near future.⁹ These new compounds, since they are based on aromatic moieties, can also generate a more stable, less sensitive, and more dense crystal.

Tetrazine-N-oxide, a high nitrogen content molecule, is one of the many nitrogen rich heterocyclic frameworks on which a number of high nitrogen content energetic materials is based. For instance, 3,3'-azobis(6-amino-1,2,4,5-tetrazine)-mixed N-oxides (DAATO_{3,5}) (structure illustrated in Fig. 1) is a tetrazine-N-oxide based nitrogen rich energetic material, which recently received increased attention due in large part to its extremely high burn rate and low dependency on pressure.^{2,6} The average oxygen content in this material

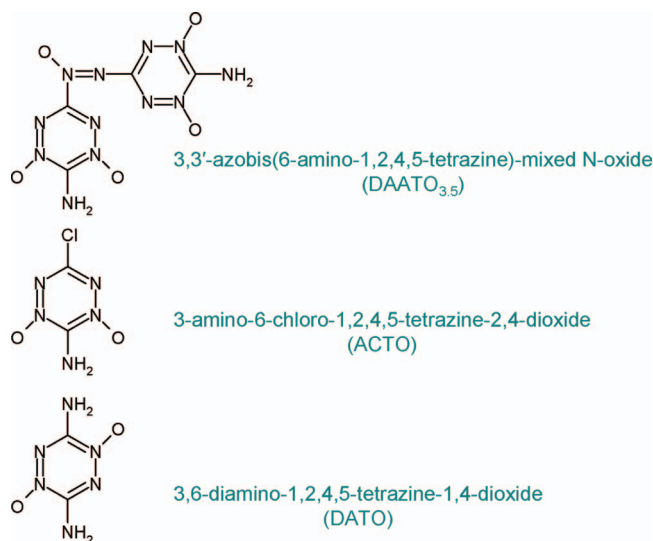


FIG. 1. Chemical structures of tetrazine-N-oxide based energetic molecules: DAATO_{3,5}, ACTO, and DATO.

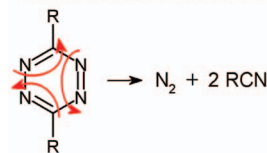
^{a)}Author to whom correspondence should be addressed. Electronic mail: erb@lamar.colostate.edu.

was determined to be about 3.5 atoms per molecule.¹ Another two important tetrazine-N-oxide based energetic molecules are 3-amino-6-chloro-1,2,4,5-tetrazine-2,4-dioxide (ACTO) (structure in Fig. 1) and 3,6-diamino-1,2,4,5-tetrazine-1,4-dioxide (DATO) (structure in Fig. 1),⁸ which have been relatively unexploited for use as energetic materials. DAATO_{3,5} and ACTO differ from DATO mainly by the relative position of the oxygen atom attached to the tetrazine ring. DAATO_{3,5} and ACTO possess a tetrazine-2,4-dioxide moiety, whereas DATO has a tetrazine-1,4-dioxide moiety.

From an energetic point of view, two potential advantages of tetrazine-N-oxides over a bare tetrazine ring can be mentioned.¹⁰ First, formation of an N-oxide of a heterocyclic ring enhances the aromaticity in the ring, which makes it less sensitive to destructive stimuli (e.g., friction). Second, N-oxides provide a better oxygen balance in energetic materials, and their alternating charges help increase the solid density by enabling better crystal packing. Except that two studies of the basic sensitivity and performance of tetrazine-N-oxide based energetic materials appeared in literature,^{2,6} however, the unimolecular decomposition of these molecules has not been studied thus far. Additionally, excited electronic states are proposed to play an important role in the shock wave decomposition of energetic materials;¹¹ excited electronic states can be created by decreasing the highest occupied molecular orbital-lowest unoccupied molecular orbital energy gap via compression from the wave front of a shock wave and by the shearing of crystal planes.¹² *Ab initio* calculations show that a compression at a pressure of 30 GPa or above causes an electronic excitation equivalent to 2–5 eV,^{13–15} which is comparable to the excitation energies of the low lying singlet excited electronic states of energetic molecules; high energy electronic states should relax rapidly to the lower energy states through internal conversion and conical intersection. Moreover, gas phase decomposition also plays an important role in the initiation process of these materials, even for the condensed phase.^{16–18} Therefore, investigation of the decomposition pathway for the isolated gas phase molecule will provide very important information for the understanding of the initiation of the combustion and detonation of these materials in condensed phase, and elucidation of detailed fundamental steps in the unimolecular decomposition of tetrazine-N-oxide based energetic molecules from their low lying excited electronic states is essential for understanding, controlling, and enhancing the detonation performances of these materials.

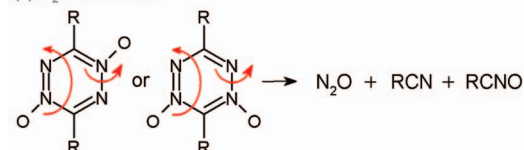
In this work, we focus on understanding the decomposition mechanisms and dynamics of DAATO_{3,5}, DATO, and ACTO under molecular beam conditions. Thus far, NO is experimentally observed to be an initial decomposition product from their excited electronic states; nonetheless, we do not exclude the possibility of generating N₂ as another initial decomposition product from these molecules. The NO product is rotationally cold (20 K), but vibrationally hot (1200 K), for tetrazine-2,4-oxide based molecules such as DAATO_{3,5} and ACTO, while the NO product is rotationally hot (50 K), but vibrationally cold [only (0–0) transition of NO is observed], for tetrazine-1,4-dioxide based molecules such as DATO. Therefore, the relative position of the oxygen

• Tetrazine Based Molecules:

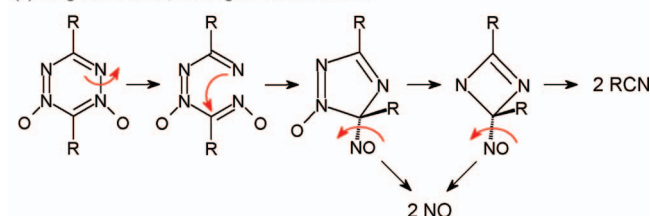


• Tetrazine-N-oxides Based Molecules:

(a) N₂O elimination



(b) Ring contraction, leading to NO elimination



(c) Meisenheimer rearrangement, leading to N₂ elimination

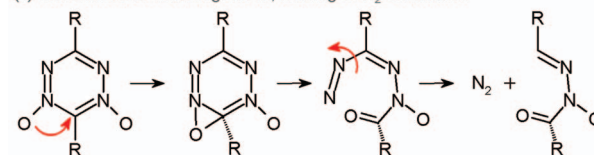


FIG. 2. Different possible decomposition pathways of tetrazine and tetrazine-N-oxide based molecules.

atoms attached to the tetrazine ring evidences a significant effect on the final internal energy distribution among products following excited electronic state decomposition of tetrazine-N-oxide based energetic molecules.

DAATO_{3,5}, ACTO, and DATO are N-oxide derivatives of the tetrazine aromatic heterocyclic ring. Photodissociation of the tetrazine molecule has been intensively investigated both experimentally and theoretically.^{19–21} To date, N₂ is undoubtedly corroborated to be the initial photodecomposition product (see Fig. 2); however, different experiments support different mechanisms (either concerted or stepwise) for this photodissociation reaction. Considering a similar decomposition mechanism, the immediate discernible photodissociation product for tetrazine-N-oxides is predicted to be N₂O (see Fig. 2), which in principle could be an intermediate precursor for the NO product observed in the experiment. Thus, a comparison of the rotational and vibrational distributions of the NO product from photolysis of N₂O to that from photolysis of DAATO_{3,5}, ACTO, and DATO is performed, so that one can determine whether N₂O could be an appropriate intermediate in the excited electronic state decomposition of these molecules. Experimentally, we confirm that N₂O is not an intermediate precursor for the NO product. Moreover, the decomposition behavior of tetrazine-N-oxides is different from that of the bare tetrazine ring, which produces N₂ and HCN as decomposition products through a concerted triple decomposition mechanism.^{19–21}

Ab initio calculations at the CASMP2/CASSCF level of theory are employed to explore the relevant excited electronic state potential energy surfaces and conical intersec-

tions for DATO and ACTO. Based on these calculations, and the experimental observations, we propose that a novel ring contraction mechanism through an $(S_1/S_0)_{CI}$ conical intersection is involved in the excited electronic state decomposition of tetrazine-N-oxide based molecules. The NO product is the result of this mechanism. Thus, present results provide several detailed insights into the unimolecular decomposition behavior of the tetrazine-N-oxide based energetic molecules from their excited electronic states.

II. EXPERIMENTAL METHODS

The experimental setup consists of nanosecond laser systems, a supersonic jet expansion pulsed nozzle, and a time of flight mass spectrometer (TOFMS) chamber, described in detail elsewhere.^{22–28} In this work, a single pump/probe laser beam with 8 ns time duration at three wavelengths (226, 236, and 248 nm) is used both to initiate dissociation of tetrazine-N-oxide based molecules and to detect NO following a one color (1+1) R2PI (resonance enhanced two photon ionization) scheme [$A \ ^2\Sigma(v'=0) \leftarrow X \ ^2\Pi(v''=0,1,2)$ and $I \leftarrow A$ transitions] through a TOFMS. The three UV laser wavelengths used in these experiments are generated by a pulsed dye laser, pumped by the second harmonic (532 nm) of the neodymium-doped yttrium aluminum garnet laser's fundamental output (1.064 μm), in conjunction with a nonlinear wavelength extension system. Typical pulse energy of the UV laser is 200–600 μJ /pulse depending on the exact wavelength of interest for a one-color experiment, which gives a laser beam intensity (I) ~ 1.3 to 4×10^7 W/cm^2 for an 8 ns pulse duration at a focused beam diameter of 0.5 mm.

The isolated gas phase DAATO_{3,5}, ACTO, and DATO molecules are produced through a combination of matrix assisted laser desorption (MALD) and supersonic jet expansion. The nozzle employed for the sample beam generation and the procedure for the sample drum preparation are the same as those used for our previous energetic materials experiments.^{22–25} A 1% N₂O in He gas mixture is prepared for the calibration of NO from decomposition of N₂O at the excitation wavelengths mentioned above.

The experiment is run at a repetition rate of 10 Hz. The timing sequence for the pulsed nozzle, ablation laser, and ionization laser is controlled by a time delay generator (SRS DG535). The molecular beam is perpendicularly crossed by the UV laser beam that is focused to a spot size of about 0.5 mm at the ionization region of a TOFMS. A background pressure of 1×10^{-5} Torr is maintained in the vacuum chamber during the experiment. Ion signals are detected by a microchannel plate detector. Signals are recorded and processed on a personal computer using a box car averager (SRS SR 250) and an analogue to digital conversion (ADC) card (Analog Devices RTI-800). DAATO_{3,5}, ACTO, and DATO are supplied by Los Alamos National Laboratory (D. E. Chavez) and used without additional purification.

III. THEORETICAL METHODS

Potential energy surface calculations and geometry optimizations for ACTO and DATO are performed at the

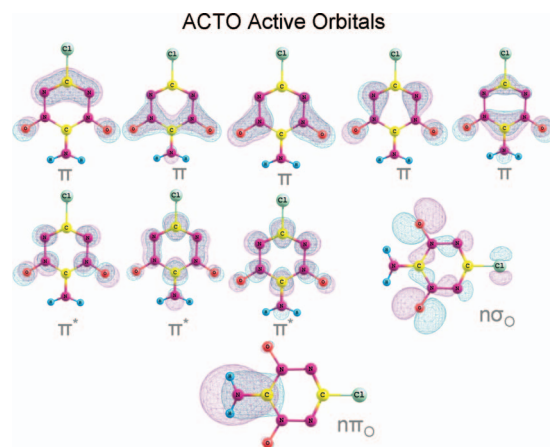


FIG. 3. Orbitals used in the active space of CASSCF calculations for ACTO. The (10,8) active space comprises only bonding and antibonding π orbitals. The (14,10) active space includes two more nonbonding orbitals.

CASSCF/6-31G(d) level of theory with the GAUSSIAN03 program.²⁹ No symmetry restrictions are applied during the calculations. For calculations on the S_1 excited state potential energy surface of DATO and ACTO, an active space comprising 14 electrons in 10 orbitals, denoted as CASSCF(14,10), is used. Orbitals used in the CASSCF(14,10) calculations are bonding π , antibonding π^* , and two nonbonding orbitals, which are shown in Fig. 3 for ACTO. Vertical excitation energies are computed by state averaging over the ground state and two successive singlet excited states with equal weights. For reliable estimation of vertical excitation energies, MP2 correlated CASSCF energies are also calculated. As the S_1 excited electronic surface for both ACTO and DATO is an (n, π^*) excited state, the active space for the optimization of the critical points (local minimum and conical intersections) on the S_1 surface should include all the bonding and antibonding π orbitals and two in-plane O nonbonding $n\sigma_O$ orbitals. The geometries of the critical points are optimized with state averaging over S_0 and S_1 states with equal weights. On the other hand, as the S_2 and S_3 excited electronic surfaces have a (π, π^*) character, critical points [local minimum, denoted as $(\pi, \pi^*)_{\text{Min}}$], and conical intersections for S_2 and S_3 are optimized with a reduced active space of (10,8), including only π bonding and antibonding orbitals. Then single point energies are calculated for these critical points on the S_2 and S_3 surfaces to obtain relative energy differences with large active space (14,10) for DATO and ACTO, respectively. Transition state structures are characterized by analytical frequency calculations. The selection of the level of theory and the active space is justified by the comparison between the calculated vertical excitation energies and experimental absorption maxima in Sec. V. The accuracies of the calculations along the reaction pathway are difficult to estimate quantitatively since we do not have any direct experimental information about the conical intersections and transition states. Calculations, however, are based on the experimental observations, including decomposition products and the energy distributions of these products, and therefore the proposed reaction pathways based on the computational results provide a reasonable and qualitative interpretation of the experimental observations. A

sensible range of values for uncertainties, based on the experimental results to which one can compare, is ± 0.5 eV.

IV. EXPERIMENTAL RESULTS

In this study, the parent molecule of interest is excited to an excited electronic state by absorption of a single UV photon at three excitation wavelengths (226, 236, and 248 nm). The parent molecules decompose into products through specific decomposition pathways. Different possible decomposition pathways of tetrazine-N-oxides based molecules are illustrated in Fig. 2. Tetrazine-N-oxide based molecules potentially can generate a number of initial products such as N_2O , NO, and N_2 through concerted or stepwise ring opening, ring contraction, and Meisenheimer rearrangement mechanisms, respectively. Nitric oxide (NO), however, is experimentally observed to be an initial dissociation product in the excited electronic state decomposition of DAATO_{3,5}, ACTO, and DATO. The NO product from decomposition of tetrazine-N-oxides is generated following single photon absorption. This is confirmed by the careful analysis of the linewidth of the NO mass peak. Extra kinetic energy from photodissociation following multiphoton absorption would generate additional linewidth for product mass channels. Moreover, if tetrazine-N-oxides absorb multiple photons at 226 nm sequentially, they can be fragmented into NO following ionization. This will also lead to a broadening of the linewidth of the NO mass signal. The linewidth of the NO mass channel signal is observed to be about 10 ns, which is the instrumental linewidth of our laser/TOFMS set up. Therefore, we believe that the NO product is associated with a single photon absorption by these molecules. Furthermore, laser beam fluence is reduced (~ 200 μJ /pulse) so that multiphoton dissociation of tetrazine-N-oxides is avoided. Excited electronic states of energetic materials that can be generated in the MALD process would be effectively relaxed and cooled in the highly collisional expansion process through the supersonic nozzle.

The NO product is probed using a one-color (1+1) R2PI detection scheme through TOFMS. The three excitation wavelengths used in this work also correspond to the resonance (0-0), (0-1), and (0-2) vibronic bands of the $A^2\Sigma^+ \leftarrow X^2\Pi$ electronic transitions of the NO product, respectively. By scanning the nanosecond laser excitation wavelength, a (1+1) R2PI rotationally resolved spectrum of the NO product from different parent molecules is recorded. The parent molecule has continuous absorption in these wavelength regions.

Although the MALD technique is a good method to place easily fragmented, fragile molecules in the gas phase without fragmentation, great effort is taken in our previous and present work to ensure that the sample molecules are not fragmented in the ablation process.²²⁻²⁵ Three different methods have been employed to explore this issue: comparison of NO velocity distributions from the nozzle, determination of arrival time for the NO signal intensity as a function of nozzle/pump laser timing, and NO rotational and vibrational temperature determinations as a function of NO source.

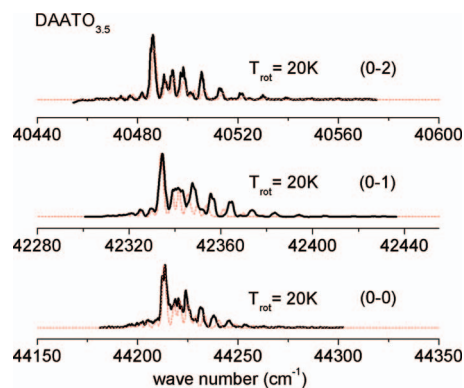


FIG. 4. One color (1+1) R2PI spectra of the vibronic transitions $A^2\Sigma^+(v'=0) \leftarrow X^2\Pi(v''=0,1,2)$ of the NO product from the excited electronic state decomposition of DAATO_{3,5}. Rotational temperature simulations with a Boltzmann population distribution show that the three observed vibrational levels on the ground electronic state have a similar rotational temperature of ca. 20 K.

These methods demonstrate that NO from DAATO_{3,5} is generated at the ionization region of the TOFMS, not in the laser desorption region of the nozzle.

(1+1) R2PI spectra of the three vibronic transitions, $A^2\Sigma^+(v'=0) \leftarrow X^2\Pi(v''=0,1,2)$ of the NO product observed from excited electronic state decomposition of DAATO_{3,5} are shown in Fig. 4. The most intense feature in each spectrum of NO can be assigned as the ($Q_{11}+P_{12}$) band head of each vibronic band,³⁰ and the less intense features within each spectrum are due to other rovibronic transitions. Spectral simulations based on Boltzmann population distributions for the three vibronic transitions produce similar rotational temperatures (~ 20 K). The vibrational temperature of the NO product from DAATO_{3,5} can also be obtained by simulating the relative intensities among the observed vibronic bands using a Boltzmann population distribution analysis and Franck-Condon (FC) factors. By comparing the experimental data with simulations at different vibrational temperatures, the vibrational temperature of the NO product from DAATO_{3,5} is estimated to be 1200 K.

Similar (1+1) R2PI spectra of three vibronic transitions, $A^2\Sigma^+(v'=0) \leftarrow X^2\Pi(v''=0,1,2)$ of the NO molecule obtained from excited electronic state decomposition of ACTO are shown in Fig. 5. The (0-0), (0-1), and (0-2) vibronic bands of the NO product from ACTO show similar rotational patterns to those of the NO product from DAATO_{3,5}, and the rotational temperature of these bands is also about 20 K.

The excited electronic state decomposition of the DATO also generates a NO product, however, with only a $v''=0$ population. The (1+1) R2PI spectrum of the (0-0) vibronic band of the NO product from DATO is illustrated in Fig. 6, which shows a hotter rotational pattern with a temperature of about 50 K. Thus, distinctly different rovibrational distributions of the NO product are observed from DATO and ACTO. The major structural difference between these two molecules is the relative position of the oxygen atoms attached to the tetrazine ring. Therefore, the relative position of oxygen atoms in tetrazine-N-oxide based energetic molecules is proposed to play an important role in their energetic and explosive behavior.

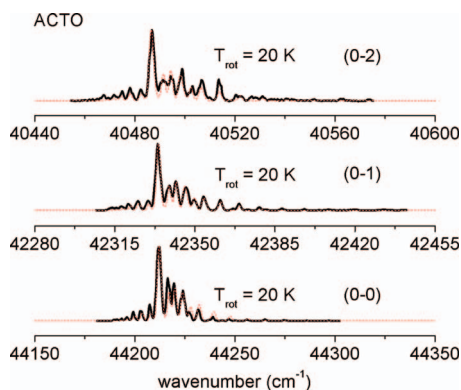


FIG. 5. One color (1+1) R2PI spectra of the vibronic transitions $A^2\Sigma^+(v'=0) \leftarrow X^2\Pi(v''=0, 1, 2)$ of the NO product from the excited electronic state decomposition of ACTO. Rotational temperature simulations with a Boltzmann population distribution show that the three observed vibrational levels on the ground electronic state have a similar rotational temperature of ca. 20 K.

(1+1) R2PI spectrum of NO from photolysis of N_2O in the NO $A^2\Sigma^+(v'=0) \leftarrow X^2\Pi(v''=0)$ transition region is presented in Fig. 7. Only the (0-0) vibronic band of the NO product is observed from photolysis of N_2O at 226 nm photoexcitation, and the spectrum is characterized by a rotational temperature of about 150 K. Assuming N_2O is an intermediate precursor for the NO product in the excited electronic state decomposition of tetrazine-N-oxide based molecules, the final NO product should present similar or hotter rotational or vibrational distributions compared to that from N_2O gas, which is cooled before photolysis under molecular beam conditions. NO from photolysis of all tetrazine-N-oxide based energetic molecules is, however, rotationally colder and vibrationally hotter than, or similar to, that from N_2O gas. These differences indicate that N_2O cannot be an intermediate precursor for the NO product in the excited electronic state decomposition of tetrazine-N-oxides. Instead, a ring contraction mechanism is proposed to be the mechanism of NO elimination from these molecules. Furthermore, one can also infer that excited electronic state decomposition behavior of tetrazine-N-oxide is essentially different from that of bare tetrazine.

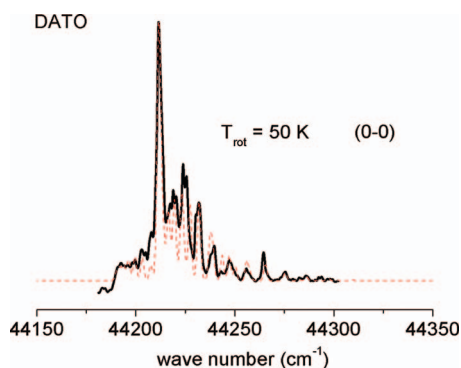


FIG. 6. One color (1+1) R2PI spectra of the vibronic transitions $A^2\Sigma^+(v'=0) \leftarrow X^2\Pi(v''=0)$ of the NO product from the excited electronic state decomposition of DATO. Rotational temperature is estimated to be ca. 50 K.

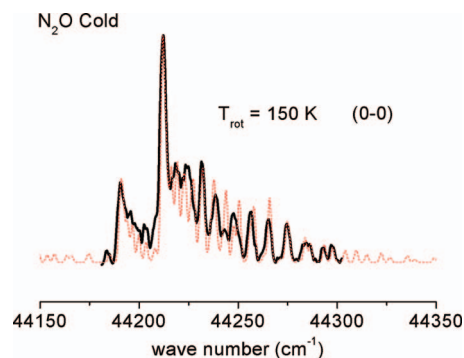


FIG. 7. One color (1+1) R2PI spectra of the vibronic transitions $A^2\Sigma^+(v'=0) \leftarrow X^2\Pi(v''=0)$ of the NO product from the excited electronic state decomposition of N_2O . Rotational temperature is estimated to be ca. 150 K.

V. THEORETICAL RESULTS

For the assessment of which excited electronic states of tetrazine-N-oxide based molecules are relevant to our experimental observations, a comparison between the computed vertical excitation energies and experimental excitation energies is performed. The vertical excitation energies (E_{vert}) for ACTO, computed at the CASSCF(10,8)/6-31G(d) optimized FC geometry (FC geometry at ground state minimum) of C_1 symmetry including only bonding and antibonding π orbitals in the active space, are listed in Table I. The CASSCF calculations show that the three lowest lying excited electronic states (S_1 , S_2 , and S_3) for ACTO possess vertical excitation energies of 3.87, 5.14, and 5.9 eV, respectively. The calculated vertical excitation energies of the S_2 and S_3 states at the MP2 correlated CASSCF level of theory are 4.59 and 5.52 eV, respectively, which are in good agreement with the experimental absorption maxima of 4.14 and 5.5 eV (see Figure S1 of supporting information for UV-visible absorption spectrum of ACTO);³¹ however, the calculated vertical

TABLE I. Calculated vertical excitation energies (E_{vert}) and relative energies of the conical intersections and transition states (ΔE) with respect to the energy of FC geometry, optimized at CASSCF(10,8)/6-31G(d).

Compound	State/CI	Configurations	$E_{\text{vert}}/\Delta E$ (eV) ^a	E_{vert} (Expt., eV) ^b
ACTO	S_1 (FC)	(n, π^*)	3.87(3.80)	2.91
	S_2 (FC)	(π, π^*)	5.14(4.59)	4.14
	S_3 (FC)	(π, π^*)	5.90(5.52)	5.50
	$(S_1/S_0)_{\text{CI}}$		2.45	
	$(S_2/S_1)_{\text{CI}}$		4.85	
	$(S_3/S_2)_{\text{CI}}$			
	TS(S_0)		2.80	
DATO	S_1 (FC)	(n, π^*)	3.56(3.55)	2.72
	S_2 (FC)	(π, π^*)	4.79(4.45)	4.58
	S_3 (FC)	(π, π^*)	6.18(5.92)	6.17
	$(S_1/S_0)_{\text{CI}}$		2.50	
	$(S_2/S_1)_{\text{CI}}$		2.81	
	TS(S_0)			
	TS(S_1)			

^aNumbers within brackets give the MP2 correlated CASSCF energies (eV).
^bExperimental absorption maxima for each compound obtained from UV-visible absorption spectra [see Fig. S1 in supporting information, Ref. 31].

excitation energy (3.8 eV) of the S_1 state even at MP2 correlated CASSCF level of theory is in poor agreement with the experimental absorption maximum of 2.9 eV. In order to improve the calculation for the vertical excitation energy associated with S_1 state, a larger (14,10) active space including two more nonbonding orbitals is necessary. The vertical excitation energy of the S_1 state at the CASSCF(14,10)/6-31G(d) level of theory is calculated to be 3.4 eV, which is in better agreement with the experimental absorption maximum of 2.9 eV. The calculated vertical excitation energies for S_2 and S_3 states change slightly with a (14,10) active space. In addition, calculation at the CASSCF(14,10)/6-31G(d) level of theory also shows that the S_1 state includes significant mixing between (n, π^*) and (π, π^*) configurations. The relative weights of the (π, π^*) and (n, π^*) configurations to the S_1 state are computed to be 30% and 70%, respectively. The calculated vertical excitation energies of the S_2 and S_3 states for DATO (see Table I) at both CASSCF and MP2 correlated CASSCF(10,8) levels of theory are also in good agreement with the experimental absorption maxima; however, considerable mismatch also exists between theory and experiment for vertical excitation energy of S_1 state. The disagreement between experiment and theory is around 0.5 eV, which falls into the commonly acceptable uncertainty range of ± 0.5 eV. Since the calculated excitation energies are compared to the methanol solution phase absorption data, a good part of this 0.5 eV “accuracy range” may be associated with solvent and intermolecular interaction effects which are present in solution.

Therefore, the CASSCF computation including only bonding and antibonding π orbitals in the active space provides a reasonable treatment of the S_3 and S_2 excited electronic states; however, inclusion of nonbonding orbitals ($n\sigma_O$ and $n\pi_N$) in the active space is necessary to explore the S_1 potential energy surface of ACTO and DATO. Moreover, dynamical correlation (omitted in a CASSCF calculation but included in MP2 correlated CASSCF calculation) is not a major contributor to the low-lying excited electronic states of ACTO and DATO.

Comparison of the experimental excitation energies (5.5 eV at 226 nm, 5.26 eV at 236 nm, and 5.00 eV at 248 nm) used in this work with the calculated vertical excitation energies at the MP2 correlated CASSCF level of theory indicates that these UV-photoexcitations of ACTO and DATO primarily populate the FC modes of the S_3 or S_2 surface. A schematic one-dimensional projection of the multidimensional singlet potential energy surfaces (S_0 , S_1 , S_2 , and S_3) of ACTO with locations and structures of different critical points and conical intersections following the ring contraction pathway is plotted in Fig. 8. Following vertical excitation to the FC point of the S_3 surface, ACTO can undergo rapid nonadiabatic internal conversion from S_3 to S_2 through the $(S_3/S_2)_{CI}$ and thereafter, from S_2 to S_1 through the $(S_2/S_1)_{CI}$ conical intersection. These nonadiabatic state changes occur without significant change in nuclear configuration (molecular geometry). This process is energetically accessible from the FC point of the S_3 surface, because practically no barriers exist along the minimum energy pathway for this process.

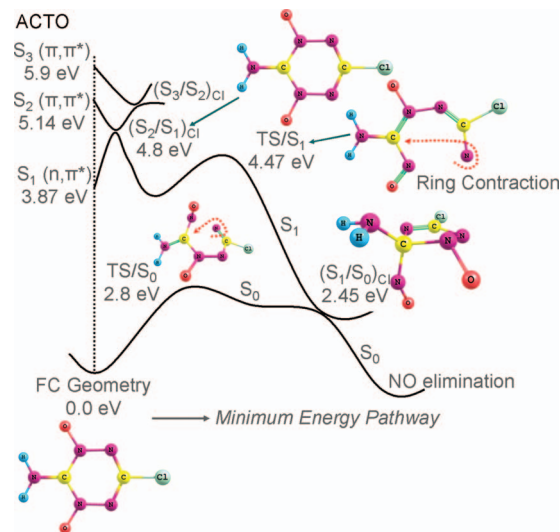


FIG. 8. One dimensional projection of the multidimensional singlet electronic potential energy surfaces of ACTO computed at CASSCF(10,8)/6-31G(d) level of theory. Geometry near the $(S_1/S_0)_{CI}$ supports a ring contraction mechanism for excited electronic state decomposition of ACTO, which finally results in NO elimination. Note that ring contracted form of ACTO near the $(S_1/S_0)_{CI}$ has a nearly linear C–NO moiety attached to the triazole ring, which can finally generate a rotationally cold NO product.

Following internal conversion to the S_1 surface, under isolated molecular beam conditions, the excitation energy is stored in the vibrational degrees of freedom of the molecule on the S_1 surface. Therefore, a ring contraction excited electronic state process can be initiated on the S_1 surface of ACTO. On the S_1 surface, the activation barrier (at 4.47 eV with respect to the S_0 FC point, see Fig. 8) for ring contraction of ACTO can easily be surmounted because the excess energy stored in the vibrational degrees of freedom of the S_1 molecule, following radiationless internal conversion of the ACTO to the S_1 surface, is sufficient to surmount the barrier. Following this transition state, the molecule is directed to the $(S_1/S_0)_{CI}$ and relaxes back to S_0 surface upon which NO elimination takes place with no activation barrier. Thereby, in brief, the ring contraction of the electronically excited ACTO, which leads to the formation of ground state NO as an initial decomposition product, begins on the S_1 surface and develops through the $(S_1/S_0)_{CI}$.

A similar one-dimensional projection of the multidimensional singlet potential energy surfaces (S_0 , S_1 , and S_2) of DATO with locations and structures of different critical points and conical intersections following the ring contraction pathway is plotted in Fig. 9. Following vertical excitation to the FC point of the S_2 surface, DATO can undergo rapid nonadiabatic internal conversion from S_2 to S_1 through the $(S_2/S_1)_{CI}$ conical intersection. This internal conversion to the S_1 surface, under isolated molecular beam conditions, stores the remainder of the excitation energy in the vibrational degrees of freedom of the molecule on the S_1 surface, which can initiate a ring contraction excited electronic state process. Following the ring contraction transition state, the molecule is directed to the $(S_1/S_0)_{CI}$ and relaxes back to the S_0 surface upon which NO elimination takes place with no activation barrier.

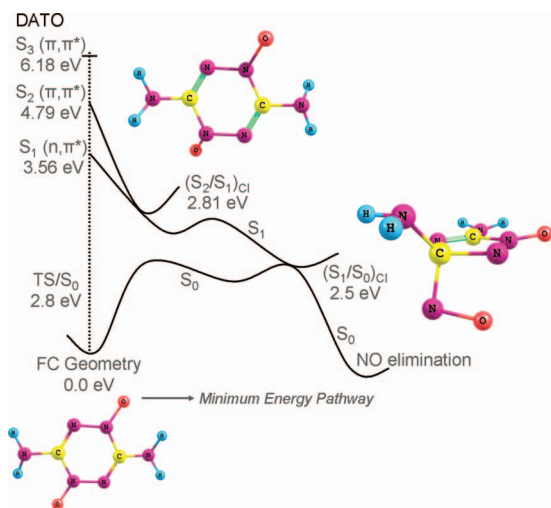


FIG. 9. One dimensional projection of the multidimensional singlet electronic potential energy surfaces of DATO computed at CASSCF(10,8)/6-31G(d) level of theory. Geometry near the $(S_1/S_0)_{CI}$ supports a ring contraction mechanism for excited electronic state decomposition of DATO, which finally results in NO elimination. Note that ring contracted form of DATO near the $(S_1/S_0)_{CI}$ has a bent C–NO moiety attached to the triazole ring, which can finally generate a rotationally hot NO product.

VI. DISCUSSION

NO product is observed from all the tetrazine-N-oxide based molecules studied in the present work. The NO product from DAATO_{3,5} and ACTO displays similar cold rotational (20 K) and hot vibrational distributions (1200 K). DATO, on the other hand, renders hotter (50 K) rotational and colder [only (0-0) transition of NO is observed] vibrational distributions for the NO product. DAATO_{3,5} and ACTO differ from DATO primarily by the relative position of oxygen atoms attached to the tetrazine ring. Thus, we propose that the relative position of oxygen atoms in tetrazine-N-oxides will have significant effect on their energetic behavior: one of these O–N attachments could presumably be superior to the other with regard to the overall energetic properties of these systems.

Comparison of the rotational and vibrational distributions of the NO product from excited electronic state decomposition of N₂O to those of DAATO_{3,5}, ACTO, and DATO suggests that N₂O could not be an intermediate precursor for the NO product observed in the experiment. These results preclude an N₂O elimination pathway involved in the excited electronic state decomposition of tetrazine-N-oxide based molecules. Furthermore, this comparison shows that the excited electronic state decomposition of tetrazine-N-oxides evolves through a different mechanism than that of bare tetrazines, which are shown to decompose through a concerted triple dissociation mechanism leading to N₂ elimination.^{19–21}

An N₂ product, however, can be generated from tetrazine-N-oxides through Meisenheimer rearrangement (see Fig. 1). Currently, we started (2+1) REMPI experiments at 203 nm for the detection of N₂ from these nitrogen rich molecules.³²

The theoretical results show that a ring contraction mechanism is involved in generation of an NO product from excited electronic state decomposition of ACTO and DATO. Ring contraction takes place near the $(S_1/S_0)_{CI}$ conical inter-

section as these molecules evolve from low lying excited electronic states. Our past studies on energetic materials firmly established that conical intersections (due to breakdown of the Born–Oppenheimer approximation leading to the crossing of two adiabatic Born–Oppenheimer surfaces) are central features in the excited electronic state decomposition of energetic molecules.^{25,26} Decomposition dynamics of energetic materials are purely nonadiabatic in nature. One of the most important implications of a conical intersection is rapid and efficient internal conversion from upper to lower electronic state surfaces through radiationless transition.³³ This internal conversion facilitates rapid conversion of electronic energy (produced from an initiation pulse), belonging to the upper electronic state, to vibrational energy of the lower electronic state, with a potential time scale of a few femtoseconds. Therefore, the presence of conical intersections for the ring contraction reaction pathway of tetrazine-N-oxides suggests that initial NO elimination in the excited electronic state decomposition of tetrazine-N-oxides is ultrafast.

As mentioned above, the major structural difference between ACTO and DATO is the relative position of oxygen atoms attached to the tetrazine ring (2,4 versus 1,4). Although a ring contracted geometry is optimized for both ACTO and DATO near the $(S_1/S_0)_{CI}$ conical intersection, one can notice a subtle difference in the geometry between ACTO and DATO, which can well explain the different energy distributions for the NO products from these two molecules. As shown in Figs. 8 and 9, the C–NO moiety attached to the five membered triazole ring is nearly linear ($\angle CNO \sim 150^\circ$) for ACTO, but is clearly bent ($\angle CNO \sim 95^\circ$) for DATO. The nearly linear C–NO moiety attached to the ring contracted form of ACTO near $(S_1/S_0)_{CI}$ probably exerts less torque on the terminal NO moiety than does the ring contracted form of DATO during the NO elimination process. This explains the observation of a rotationally cold (20 K) product for excited electronic state decomposition of ACTO. A bent C–NO moiety, on the other hand, attached to the ring contracted form of DATO near $(S_1/S_0)_{CI}$ can exert considerable torque on the terminal NO moiety during the NO elimination process. This $(S_1/S_0)_{CI}$ geometry difference explains the observation of rotationally hotter (50 K) distributions of the NO product from DATO.

Theoretical prediction for DAATO_{3,5} is not possible at the CASSCF level of theory with a balanced active space; however, similar rovibrational spectral structures for the NO product observed in the experiment for both DAATO_{3,5} and ACTO indicate that decomposition of DAATO_{3,5} evolves through a similar ring contraction mechanism.

VII. CONCLUSIONS

Present work on the unimolecular decomposition of tetrazine-N-oxide based high nitrogen content energetic molecules from their excited electronic states leads to a number of conclusions as following: (1) nitric oxide (NO) is observed to be an initial decomposition product from DAATO_{3,5}, ACTO, and DATO; (2) excited electronic state decomposition of DAATO_{3,5}, and ACTO produces a vibra-

tionally hotter ($T_{\text{vib}} \sim 1200$ K), but rotationally colder ($T_{\text{rot}} \sim 20$ K) fragment NO product compared to that from DATO, which generates a vibrationally colder [only (0-0) transition of NO is observed], but rotationally hotter ($T_{\text{rot}} \sim 50$ K) NO product; (3) the relative positions of the oxygen atoms attached to the ring have significant effect on the final energy distribution among product molecules following decomposition of tetrazine-N-oxide based molecules; (4) decomposition behavior of N-oxides of tetrazine based molecules is different from that of the unsubstituted tetrazine molecule, and N_2O is not an intermediate precursor of the NO product; and (5) theoretical calculation shows that an $(S_1/S_0)_{\text{CI}}$ conical intersection is involved in the excited electronic state decomposition of N-oxide based energetic molecules and that the NO product is generated through a ring contraction mechanism.

The cold vibrational distribution of the NO product from DATO decomposition reaction suggests that DATO would be a better energetic material than ACTO or $\text{DAATO}_{3,5}$ because potentially more energy can be partitioned in translational degrees of freedom for the products. This, of course, would depend to some extent on how the additional vibrational energy is distributed among all the decomposition products of the energetic material. Furthermore, these high nitrogen content energetic materials decompose from the excited electronic states in a fashion similar to that found for nitramine energetic materials; that is, through series of conical intersections to their ground electronic states. All these energetic molecules then decompose to yield NO from their highly vibrationally excited S_0 states.

The decomposition pathway determined for the isolated gas phase energetic molecule provides very important information for the understanding of the initiation of the combustion and detonation of these materials in the condensed phase. Unimolecular processes must be the first step in any decomposition process and gas phase molecules are known to be part of the overall energy release phenomenon even for condensed phase systems.

ACKNOWLEDGMENTS

We thank Dr. David E. Chavez (LANL) for sending us samples of these and many other energetic materials and their model compounds, and we thank the U.S. ARO for support of this work.

- ¹G. Steinhauser and T. M. Klapotke, *Angew. Chem., Int. Ed.* **47**, 3330 (2008).
- ²D. E. Chavez, B. C. Tappan, M. A. Hiskey, S. F. Son, H. Harry, D. Montoy, and S. Hagelberg, *Propellants, Explos., Pyrotech.* **29**, 209 (2004).
- ³D. E. Chavez, M. A. Hiskey, and R. D. Gilardi, *Angew. Chem., Int. Ed.* **39**, 1791 (2000).

- ⁴J. Neutz, O. Grosshardt, S. Schaufele, H. Schuppler, and W. Schweikert, *Propellants, Explos., Pyrotech.* **28**, 181 (2003).
- ⁵K. O. Christe, W. W. Wilson, J. A. Sheehy, and J. A. Boatz, *Angew. Chem., Int. Ed.* **38**, 2004 (1999); M. I. Eremets, A. G. Gavriluk, I. A. Trojan, D. A. Dzivenko, and R. Boehler, *Nature Mater.* **3**, 558 (2004).
- ⁶D. E. Chavez, M. A. Hiskey, M. H. Huynh, D. L. Naud, S. F. Son, and B. C. Tappan, *J. Pyrotech.* **23**, 70 (2006).
- ⁷R. P. Singh, H. Gao, D. T. Meshri, and J. M. Shreeve, *Struct. Bonding (Berlin)* **125**, 35 (2007).
- ⁸D. E. Chavez and M. A. Hiskey, *J. Energ. Mater.* **17**, 357 (1999).
- ⁹J. Bottaro, in *Overviews of Recent Research on Energetic Materials*, edited by R. W. Shaw, T. B. Brill, and D. L. Thompson (World Scientific, Singapore, 2004), pp. 473–501.
- ¹⁰K. Yamaguchi, H. Takahashi, T. Kaihoh, T. Itoh, M. Okada, K. Nagata, G. Matsumura, and A. Ohsawa, *Acta Crystallogr., Sect. C: Cryst. Struct. Commun.* **48**, 1237 (1992).
- ¹¹*Overviews of Recent Research on Energetic Materials*, edited by R. W. Shaw, T. B. Brill, and D. L. Thompson (World Scientific, Singapore, 2004), pp. 161–189.
- ¹²J. J. Gilman, *Philos. Mag. B* **71**, 1057 (1995).
- ¹³M. M. Kuklja, B. P. Aduiev, E. D. Aluker, V. I. Krashenin, A. G. Krechetov, and A. Y. Mitrofanov, *J. Appl. Phys.* **89**, 4156 (2001).
- ¹⁴M. M. Kuklja, E. V. Stefanovich, and A. B. Kunz, *J. Chem. Phys.* **112**, 3417 (2000).
- ¹⁵A. V. Kimmel, P. V. Sushko, A. L. Shluger, and M. M. Kuklja, *J. Chem. Phys.* **126**, 234711 (2007).
- ¹⁶J. Sharma and B. C. Beard, *Mater. Res. Soc. Symp. Proc.* **296**, 189 (1993).
- ¹⁷T. R. Botcher, H. D. Landouceur, and T. R. Dussel, "Shock Compression of Condensed Matter-1997," Proceedings of the Conference of the APS Tropical Group, 1998 (unpublished), Vol. 429, p. 989.
- ¹⁸B. P. Aduiev, E. D. Aluker, and A. G. Krechetov, *Chem. Phys. Rep.* **17**, 469 (1998).
- ¹⁹G. E. Scuseria and H. F. Schaefer, *J. Phys. Chem.* **94**, 5552 (1990).
- ²⁰X. Zhao, W. B. Miller, E. J. Hints, and Y. T. Lee, *J. Chem. Phys.* **90**, 5527 (1989).
- ²¹A. C. Scheiner, G. F. Scuseria, and H. F. Schaefer, *J. Am. Chem. Soc.* **108**, 8160 (1986); L. Nahon and P. Morin, *J. Am. Chem. Soc.* **96**, 3628 (1992).
- ²²H.-S. Im and E. R. Bernstein, *J. Chem. Phys.* **113**, 7911 (2000).
- ²³Y. Q. Guo, M. Greenfield, and E. R. Bernstein, *J. Chem. Phys.* **122**, 244310 (2005).
- ²⁴Y. Q. Guo, M. Greenfield, A. Bhattacharya, and E. R. Bernstein, *J. Chem. Phys.* **127**, 154301 (2007).
- ²⁵Y. Q. Guo, A. Bhattacharya, and E. R. Bernstein, *J. Chem. Phys.* **128**, 034303 (2008).
- ²⁶A. Bhattacharya, Y. Q. Guo, and E. R. Bernstein, *J. Phys. Chem. A* **113**, 811 (2009).
- ²⁷M. Foltin, G. J. Stueber, and E. R. Bernstein, *J. Chem. Phys.* **114**, 8971 (2001).
- ²⁸M. Foltin, G. J. Stueber, and E. R. Bernstein, *J. Chem. Phys.* **111**, 9577 (1999).
- ²⁹M. J. Frisch, G. W. Trucks, H. B. Schlegel *et al.*, GAUSSIAN 03, Revision B.04, Gaussian Inc., Pittsburgh, PA, 2003.
- ³⁰M. Hippler and J. Pfab, *Chem. Phys. Lett.* **243**, 500 (1995); G. Herzberg, *Spectra of Diatomic Molecules* (Van Nostrand, New York, 1950), p. 257.
- ³¹See EPAPS supplementary material <http://dx.doi.org/10.1063/1.3262688> for absorption spectra of ACTO and DATO.
- ³²T. F. Hanisco and A. C. Kummel, *J. Phys. Chem.* **97**, 7242 (1993); W. L. Glab and J. P. Hessler, *Appl. Opt.* **26**, 3181 (1987).
- ³³A. Migani and M. Olivucci, in *Conical Intersections: Electronic Structure, Dynamics and Spectroscopy*, Advanced Series in Physical Chemistry, edited by W. Domcke, D. R. Yarkony, and H. Koppel (World Scientific, Singapore, 2004), p. 271.